

Received July 7, 2021, accepted August 11, 2021, date of publication August 16, 2021, date of current version August 30, 2021.

Digital Object Identifier 10.1109/ACCESS.2021.3105103

A Novel Design Method of LCC-S Compensated Inductive Power Transfer System Combining Constant Current and Constant Voltage Mode via Frequency Switching

WENBO WANG¹, JUNJUN DENG¹, (Member, IEEE), DELIANG CHEN¹,
ZHENPO WANG¹, AND SHUO WANG¹, (Member, IEEE)

National Engineering Laboratory for Electric Vehicles, Beijing Institute of Technology, Beijing 100081, China

Corresponding author: Junjun Deng (dengjunjun@bit.edu.cn)

This work was supported by the National Key Research and Development Program of China under Grant 2019YFE0104700.

ABSTRACT Inductive power transfer (IPT) is an attractive wireless power charging option in many applications such as electric vehicle biomedical devices and consumer electronics, etc. Constant current and constant voltage (CC-CV) charging profile is widely used for charging applications due to affecting the life and the reliability of the Li-ion battery. However, the IPT systems that can achieve both CC and CV modes with soft switching are not well studied. This paper presents an inductive power transfer system for wireless charging without a back-end converter, which achieves the required two-stage charging profile with high efficiency by keeping inverters' soft switching operation. The characteristics of an LCC-S compensation topology have been investigated thoroughly. Two fixed resonant frequencies, whose analytical expressions have been derived, can be found to realize constant current output and constant voltage output respectively under zero-phase angle condition. Besides, an effective tuning method has been presented for zero voltage switching realization to reduce the switching loss. Moreover, a parameter design procedure has been summarized for the wireless charger with a simplified structure and high efficiency. Finally, the method is validated through experiments on a 3.5kW prototype realizing constant current and constant voltage outputs with a peak efficiency of 97.3%.

INDEX TERMS Inductive power transfer, LCC-S compensation, constant current and constant voltage charging mode.

I. INTRODUCTION

IPT has received significant focus in recent years due to its advantages of safety and convenience. It has been used in fields such as wireless charging of mobile phone and electric toothbrushes in consumer electronics [1], and wireless supply to implantable devices in medical apparatus [2]. Furthermore, wireless battery charger has been designed for electric vehicle (EV) in higher power applications [3], [4].

In the above-mentioned applications, the lithium-ion (Li-ion) battery has been widely adopted due to their characteristic in terms of high energy density, compact size, and reliability [5], [6]. To charge the Li-ion batteries, there are at least two stages named constant current (CC) charge and con-

stant voltage (CV) charge [7]. Generally, the battery charging process starts with a CC mode and the battery voltage starts to rise. When the voltage rises to a specific level, the charging process is shifted to the CV mode. Subsequently, the charging process ends when the charging current decreases to a certain value. To prolong the battery life and ensure the reliability, the output voltage and current curve of the charger should be regulated accurately according to the battery charging profile, which is usually taken for granted but given less attention in conducted charging scenario. However, it is not easy to design an IPT based wireless charger that can implement a CC-CV charging profile due to the wide range of load variations.

In an IPT based wireless charging system, three components are commonly seen including high frequency (HF) inverter, the loosely magnetic coupler, and the compensation networks [8]. The compensation networks are especially

The associate editor coordinating the review of this manuscript and approving it for publication was Dušan Grujić¹.

crucial to the overall performance because it forms the resonant tanks with the loosely coupled inductors to reduce the VA rating of the system while improving the power transfer capability. Additionally, the equivalent load of the battery varies throughout the charging process affecting the value of the input impedance, which will influence the performance of the entire system. By means of the compensation topology design, the input impedance can be resistive regardless of load thus achieving zero phase angle (ZPA). In this case, the reactive power within the resonant circuit is minimized during the entire charging process, which reduces the switching loss of the HF inverter.

In general, there are four basic capacitive compensation topologies, depending on the way of the compensation capacitors being connected, namely series-series (SS), series-parallel (SP), parallel-series (PS), and parallel-parallel (PP) [9]. High-order symmetrical compensation topologies formed by LCL and LCC networks are promoted due to their superior performance [10], [11]. Additionally, the topologies adopted high order networks on the primary side and basic capacitive compensations on the secondary side have also been studied, including LCC-S, LCC-P, etc. However, the above compensation topologies are usually designed to realize either constant-current or constant-voltage output characteristic [12], which cannot match the requirement of the ideal battery charging profile. To have the wireless charger achieve both the CC and CV mode output, quantities of efforts have been carried out in recent years. Generally, these methods can be roughly divided into three categories.

1) Hybrid Compensation topologies. Since a single topology seems difficult to implement both CC and CV mode, the combination of compensation topologies with different output characteristics draw much attention, especially considering the load-independent characteristic is preferable in both modes. For example, SS and SP can achieve CC and CV outputs respectively with specific parameters, while the PS and PP can achieve load-independent CC and CV modes respectively [13]. Based on the four basic topologies, Qu *et al.* [14] and Auvigne *et al.* [15] employ a combination of two of the four basic topologies such as SS combined with PS, SP combined with PP to perform battery charging. Furthermore, high order compensation topologies are also applied in hybrid topologies. SS combining with S-LCC in [16] and LCC-LCC combining with LCC-S in [17] are proposed to realize CC and CV modes. However, changes in the working topology will inevitably require the use of several switches, which causes the extra power loss as well as complicates the control strategy. Moreover, the introduction of a hybrid circuit on the receiving side will increase the complexity of the receiving system, increase the system cost as well as reduce the portability of the system, which is contrary to the lightweight principle of the receiving side.

2) Control schemes of back-end converter or active bridges. Usually, a DC-DC converter is adopted as the back-end stage of the charger to regulate the output voltage and output current to attain the required charging profile [21]. To reduce the

number of the stages of the charging system, the phase shift control (PSC) scheme is designed and carried out by active bridges of the inverter and semi-active bridges of the rectifier to regulate the output characteristic [18]–[20]. Furthermore, variable frequency control (VFC) is proposed by the author of [22], [23] to fulfill the required output accommodating to the load. However, a back-end stage undoubtedly complicates the power circuit topology, while the complicated characteristics of the resonant tank call for the elaborated design of the PSC or the VFC scheme. Therefore, the compensation topology with both properties of load-independent CC and CV output is preferable [24], which simplifies the overall topology and the control scheme.

3) Dual-frequency switching control. As mentioned in [25], the aforementioned four basic topologies cannot implement both CC and CV modes while realizing ZPA at the same time due to limited parameter design freedom. Therefore, high order topologies have been investigated to meet this requirement. Qu and Chu [26] analyze the output characteristics of LCC-LCC by numeral calculation and realize the required load-independent CC and CV outputs at two ZPA frequencies. Nevertheless, the additional compensation capacitance and inductance introduced on the receiving side will inevitably increase the complexity and reduce the portability of the receiving side, which has the same shortcomings as the first method. To adapt to the principle of lightweight in the receiving side as well as fit the transfer characteristic, the authors of [27]–[29] realize the transformation of CC or CV mode by analyzing the characteristics of LCC-S by circuit equivalence. Analogously, the work by Lu *et al.* [30], [31] analyzes the features of high order topologies and summarizes some of the topologies that can implement CC and CV mode. However, in Lu's design method of achieving CC and CV outputs, the analytical expressions of the specifications and the design parameters do not directly link to the actual component due to the segmentation processing in the model. By way of illustration, under certain output characteristic conditions, since the relationship between self-inductance and coupling is unpredictable, the iterative coupling parameters may be impractical to implement. Meanwhile, although the ZPA constraint is handy for solving the high order resonant networks, the zero voltage switching (ZVS) is preferable for the MOSFET-based inverter. Due to the adoptions of the equivalent components to achieve parameter calculations [29]–[31], the specific ZVS tuning method are difficult to obtain, therefore, related research is still scarce. Since ZVS heavily affected the efficiency, it is necessary to explore it to improve the performance of the system. Furthermore, Table 1 is introduced in order to briefly show the difference between this work and the existing papers about LCC/S topology. It can be clearly show that this work can not only simplify the realization of CC and CV mode, but also proposes a tuning method in clearer way of ZVS which guarantees the high efficiency of system.

Focused on the LCC-S topology, aimed at solving the problem of the indecipherable relationship between

TABLE 1. Comparison between this work and existing papers about LCC-S system.

LCC/S proposed in	[27]	[28]	[29]	This work
ZPA in CV mode	YES	NO	YES	YES
ZPA in CC mode	NO	YES	YES	YES
Analysis of ZVS	YES	YES	NO	YES
Simplified system design	YES	YES	NO	YES

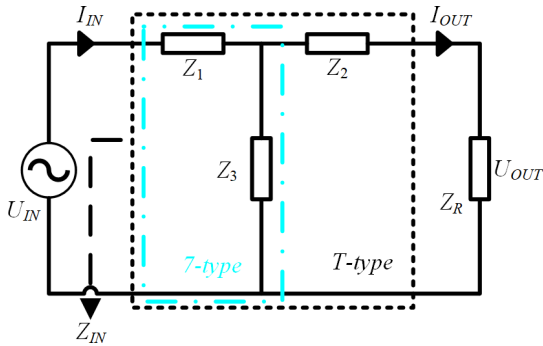


FIGURE 1. The topology of T-type and 7-type compensation.

CC-CV parameters and the unclear implementation conditions of ZVS, this paper promotes a parameter design procedure to achieve load-independent current output and load-independent voltage output while ZVS operation is guaranteed in a wide range. Firstly, the T-type and 7-type networks as two basic compensated units are introduced with their characteristics of load-independent output.

Secondly, the analytical expressions of achieving CC and CV mode for LCC-S topology have been derived respectively. Subsequently, the input impedance is analyzed for ZPA realization. Thirdly, the influence of various circuit elements on the input impedance angle is analyzed. A parameter design procedure has been proposed, which ensures the wireless charger operating at ZVS mode above 1/2 rated power in CC mode, and above 1/4 rated power in CV mode to achieve high efficiency in the entire charging process.

The rest of the paper is organized as follows. The modeling and theoretical analysis of load-independent current and voltage outputs of LCC-S compensation are mentioned in Section II. The proposed parameter design method is introduced in Section III. In section IV, both the simulation and experimental results of a 3.5kW prototype are present to validate the proposed method. Finally, Section V concludes this paper.

II. ANALYSIS OF CC AND CV MODE

A. T-TYPE AND 7-TYPE COMPENSATION NETWORKS

The T-type compensation networks as shown in Fig. 1 are widely used in circuit analysis due to the superior characteristics such as load-independent output voltage [32], [33]. According to KVL and ohm's law, we can get the following

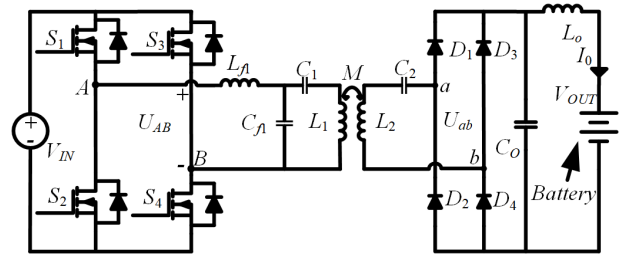


FIGURE 2. LCC-S compensation topology.

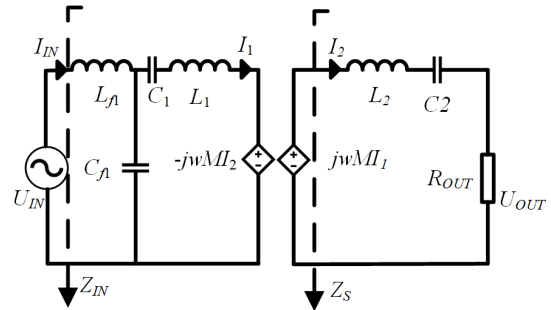


FIGURE 3. Equivalent circuit of LCC-S compensation topology.

formulas.

$$G_v = \frac{U_{OUT}}{U_{IN}} = \frac{Z_3}{(Z_1 + Z_3) + \Delta/Z_R} \quad (1)$$

$$G_i = \frac{I_{OUT}}{U_{IN}} = \frac{Z_3}{\Delta + (Z_1 + Z_3) \cdot Z_R} \quad (2)$$

where $\Delta = Z_1Z_2 + Z_1Z_3 + Z_2Z_3$, G_v is the voltage gain and G_i is the transconductance gain. From (1) and (2) separately, the condition to get the load-independent G_v and G_i are as follows:

$$\Delta = Z_1Z_2 + Z_1Z_3 + Z_2Z_3 = 0 \quad (3)$$

$$Z_1 + Z_3 = 0 \quad (4)$$

In the case of load-independent G_i , the output current characteristic is independent of Z_2 , therefore the network only consists of Z_1 and Z_3 which can be regarded as 7-type. When the input source is a sinusoidal voltage source and the above specific conditions are met, T-type and 7-type can achieve load-independent voltage output and load-independent current output respectively.

B. ANALYSIS OF LCC-S TOPOLOGY

Fig. 2 shows the LCC-S compensation topology. The circuit consist of a power supply, an inverter, a primary LCC topology and secondary S topology, a rectifier and a load network. The primary compensation network consists of resonant inductor L_{f1} , and two resonant capacitor C_{f1} and C_1 . The secondary compensation network is composed of resonant capacitor C_2 . The magnetic coupler consist of L_1 , L_2 and mutual inductance M .

For simplicity, the equivalent circuit of LCC-S is shown in Fig. 3, which is based on First Harmonic Approximation

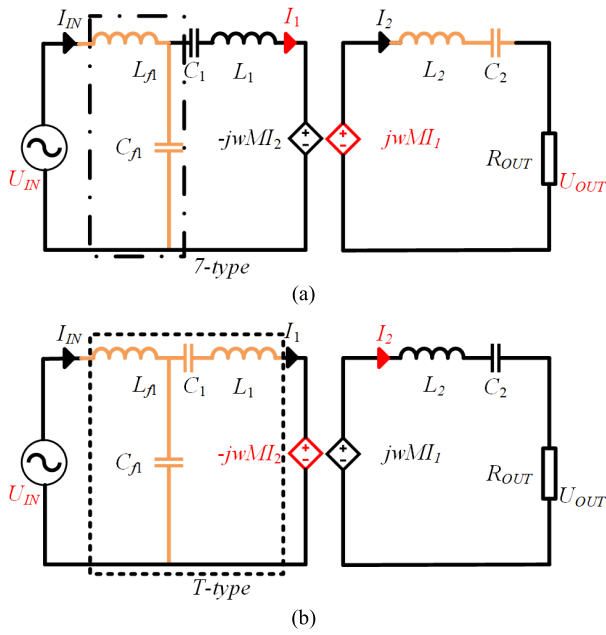


FIGURE 4. The relationship between CV and CC mode resonance parameters (a) CV mode (b) CC mode.

(FHA). Moreover, in order to facilitate the derivation of the CC mode, the CV mode, and the input impedance, the mutual inductance model is adopted. The mutual inductance can be expressed as

$$M = k\sqrt{L_1L_2} \quad (5)$$

where k is the coupling coefficient. The first harmonic components, based on the equivalent circuit in Fig. 3 can be written as

$$\begin{aligned} U_{IN} &= \frac{4}{\pi} V_{IN} \sin(\omega t), U_{OUT} = \frac{4}{\pi} V_{OUT} \sin(\omega t + \theta) \\ I_2 &= \frac{2}{\pi} I_0 \sin(\omega t + \theta), R_{OUT} = \frac{8}{\pi^2} R_r \end{aligned} \quad (6)$$

V_{AB} , V_0 , I_2 represents the value for input dc-link voltage of full bridge inverter, required voltage of battery, and required current of battery. θ is the phase between U_{IN} and U_{OUT} . R_r is the equivalent resistance of battery and R_{OUT} is the equivalent ac resistance of R_r .

C. IMPLEMENTATION OF CV MODE

The LCC network is usually designed as primary compensation for IPT system due to the simplicity of achieving a constant current through the primary coil. When the secondary coil is coupled, a stable induced voltage can be generated on the secondary side. Therefore, LCC-S topology is usually used for CV mode.

As shown in Fig. 4, the components marked in yellow are designed in specific resonance mode to meet the output characteristics. In addition, the parameters marked in red mean that they remain constant. It can be seen from Fig. 4(a) that in order to form a stable current through the primary coil,

it means that L_{f1} and C_{f1} need to form a 7-type to achieve load-independent current output, the relationship between L_{f1} and C_{f1} can be obtained as

$$j\omega_{CV}L_{f1} + \frac{1}{j\omega_{CV}C_{f1}} = 0 \quad (7)$$

Then the relationship between I_1 and U_{IN} can be calculated as

$$I_1 = \frac{U_{IN}}{j\omega_{CV}L_{f1}} \quad (8)$$

It can be seen that I_1 is only controlled by U_{IN} when L_{f1} remain unchanged. Therefore, the equivalent controlled voltage source of the secondary side ' $j\omega_{CV}MI_1$ ' is a constant value depending on U_{AB} . By applying Kirchoff's law to the Fig. 4(a), the voltage equation for the secondary circuit model can be written as

$$j\omega_{CV}MI_1 = j\omega_{CV}L_2I_2 + \frac{I_2}{j\omega_{CV}C_2} + U_{OUT} \quad (9)$$

It can be easily deduced from (9) that in order to make U_{OUT} independent of secondary parameters, L_2 and C_2 should satisfy

$$j\omega_{CV}L_2 + \frac{1}{j\omega_{CV}C_2} = 0 \quad (10)$$

When (10) is met, U_{OUT} is equal to the controlled voltage source and controlled by U_{IN} . The total voltage gain can be calculated as

$$G_v = \frac{U_{OUT}}{U_{IN}} = \frac{j\omega_{CV}MI_1}{U_{IN}} = \frac{j\omega_{CV}M \cdot U_{IN}}{U_{IN} \cdot j\omega_{CV}L_{f1}} = \frac{M}{L_{f1}} \quad (11)$$

D. IMPLEMENTATION OF CC MODE

The resonance conditions for achieving CC mode are illustrated in Fig. 4(b). Assuming that a constant load-independent current output on the secondary side has been realized, the value of the primary controlled voltage source $-j\omega_{CC}MI_2$ stays constant. In another word, the output voltage of the primary T-type compensation network is constant. In this case, according to (3) and (4), the components L_{f1} , C_{f1} and L_{e1} constituting the T-type should satisfy

$$\begin{aligned} -\omega_{CC}^2L_{f1}L_{e1} + L_{f1}/C_{f1} + L_{e1}/C_{f1} &= 0 \quad (12) \\ j\omega_{CC}L_{e1} &= j\omega_{CC}L_1 + \frac{1}{j\omega_{CC}C_1} \quad (13) \end{aligned}$$

where L_{e1} is the equivalent to L_1 and C_1 , defined as (13).

Therefore, it can be inferred from (1) and (12) that the controlled voltage source of the primary side ' $-j\omega_{CC}MI_2$ ' is a constant value depended on U_{AB} . Obviously, secondary current I_2 is directly controlled by U_{AB} . The total transconductance gain can be expressed as

$$G_i = \frac{I_{OUT}}{U_{IN}} = \frac{1}{(\omega_{CC}^2L_{f1}C_{f1} - 1)j\omega_{CC}M} \quad (14)$$

E. IMPLEMENTATION OF ZPA IN CC AND CV MODES

In order to achieve ZPA, the input impedance of the circuit needs to be calculated. The input impedance of the secondary network Z_S can be derived as

$$Z_S = j\omega L_2 + 1/j\omega C_2 + R_{OUT} \quad (15)$$

Equivalent impedance of the secondary side reflecting to primary side can be calculated as

$$Z_R = \frac{(\omega M)^2}{Z_S} \quad (16)$$

Thus the overall input impedance of the circuit can be calculated as

$$Z_{IN} = j\omega L_{f1} + \frac{1}{j\omega C_{f1}} // (j\omega L_{f1} + 1/j\omega C_{f1} + Z_R) \quad (17)$$

As shown in [27], in the condition of $Z_1 = Z_2 = -Z_3$, the input impedance is purely resistive when the load is resistor. Obviously in CV mode, the secondary side reflection impedance is resistive according to (10), (15) and (16). Moreover, (7) also satisfies $Z_1 = -Z_3$, and the ZPA can be achieved by satisfying $Z_1 = Z_2$. Therefore, conditions for implementing ZPA in CV mode can be derived as

$$\begin{cases} j\omega_{CV} L_{f1} = \frac{1}{j\omega_{CV} C_1} + j\omega_{CV} L_1 \\ \omega_{CV} = 1/\sqrt{L_{f1} C_{f1}} = 1/\sqrt{L_2 C_2} \end{cases} \quad (18)$$

As analyzed above, ZPA and CV output can be achieved by operating at a specific frequency ω_{CV} solved by (18).

However, no explicit expression of a specific frequency can be drawn directly from (12) and (13) for the CC mode to realize ZPA. In this case, the input impedance of the resonant circuit should be specially designed as resistive. To correlate the CC operating frequency with ω_{CV} , C_{f1} , C_1 , C_2 can be expressed by $1/L_{f1}\omega_{CV}^2$, $1/(L_1-L_{f1})\omega_{CV}^2$, $1/L_2\omega_{CV}^2$ according to (18). Meanwhile, the operating frequency that achieves ZPA in CC mode named ω_{CC} can be calculated from (12)(13)

$$\begin{aligned} \omega_{CC} &= \sqrt{\left(\frac{1}{L_{f1}C_{f1}} + \frac{1}{L_{e1}C_{f1}}\right)} \\ &= \sqrt{\omega_{CV}^2 + \frac{\omega_{CC}^2 L_{f1}}{\left(\frac{\omega_{CV}^2 L_1}{\omega_{CC}^2(L_1-L_{f1})} - 1\right)(L_1 - L_{f1})}} \end{aligned} \quad (19)$$

For a given primary side compensation parameter, the relationship between ω_{CC} and ω_{CV} can be expressed as

$$\omega_{CC} = \omega_{CV} \sqrt{(\delta_{1,2} + (\delta_{1,2} + L_1 - L_{f1})/L_1)/\delta_{1,2}} \quad (20)$$

where $\delta_{1,2} = L_{f1} \pm \sqrt{L_{f1}L_1}$. It is appeared that the load-independent CC output can be achieved at two frequencies, where

$$\alpha_{1,2} = \sqrt{(\delta_{1,2} + (\delta_{1,2} + L_1 - L_{f1})/L_1)/\delta_{1,2}} \quad (21)$$

The input impedance of CC mode can be calculated from (17) by submitting the ω_{CC} with $\alpha\omega_{CV}$ in (22), as shown at the bottom of the next page.

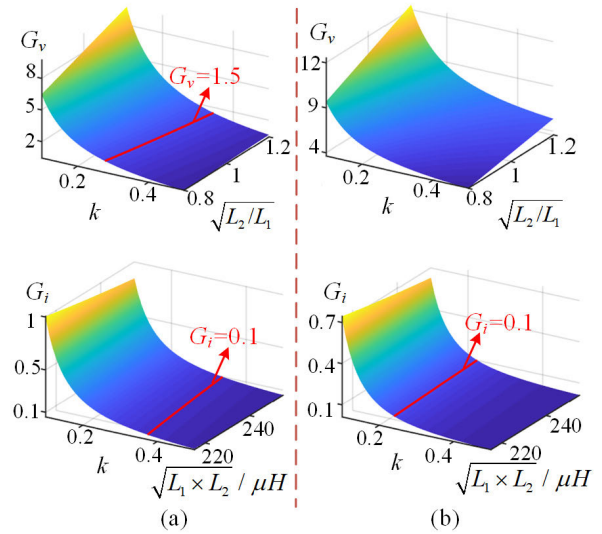


FIGURE 5. The distribution of the coupling coefficient and coupler parameters for G_v and G_i (a) case 1 (b) case 2.

In order to achieve ZPA in the CC mode, the imaginary part of Z_{inCC} needs to be zero. For case 1, $\omega_{CC1} = \alpha_1\omega_{CV}$, substituting (20) into (22) and solving, when $Im(Z_{inCC}) = 0$, L_{f1} and L_1 should satisfy

$$L_{f1,\alpha1} = L_1 \frac{k^2}{(k-1)^2} \quad (23)$$

For case 2, $\omega_{CC1} = \alpha_2\omega_{CV}$ the condition that $Im(Z_{inCC}) = 0$ can also be obtained according to the above method. Consequently, the conditions that L_{f1} and L_1 should satisfy

$$L_{f1,\alpha2} = L_1 \frac{k^2}{(k+1)^2} \quad (24)$$

Substituting (23) and (24) into (21) and simplifying, two possible cases are given as (25)

$$\begin{cases} \text{Case 1} \left\{ \begin{aligned} L_{f1,\alpha1} &= L_1 \frac{k^2}{(k-1)^2} \\ \omega_{CC1} &= \sqrt{\frac{1}{1-k}} \omega_{CV} \\ U_{OUT1} &= \frac{(1-k)^2}{k} \sqrt{\frac{L_2}{L_1}} U_{IN} \\ I_{OUT1} &= \frac{(1-k)^{3/2}}{k^2 j\omega_{CV} \sqrt{L_1 L_2}} U_{IN} \end{aligned} \right. \\ \text{Case 2} \left\{ \begin{aligned} L_{f1,\alpha2} &= L_1 \frac{k^2}{(k+1)^2} \\ \omega_{CC2} &= \sqrt{\frac{1}{1+k}} \omega_{CV} \\ U_{OUT2} &= \frac{(1+k)^2}{k} \sqrt{\frac{L_2}{L_1}} U_{IN} \\ I_{OUT2} &= \frac{(1+k)^{3/2}}{-k^2 j\omega_{CV} \sqrt{L_1 L_2}} U_{IN} \end{aligned} \right. \end{cases} \quad (25)$$

It can be clearly seen from (25) that when L_2 and L_1 are close and k is less than 1, the voltage gain of case

TABLE 2. Specification of the IPT battery charger.

Parameters	Description	Rate
P_o	Power rating	3.5kW
V_{in}	Input voltage	330DC
V_o	CV mode output voltage	400V
I_o	CC mode output current	8.75A

2 by $G_{v_case2} \approx 1/k + 2 + k > 3$ while G_{v_case1} can be less than 1. Similarly, the transconductance gain G_i of case2 is larger than that of case 1 under the same conditions. In addition, (25) indicates that if we define the equivalent load resistance at the CC/CV mode switching moment as $R_{equ} = U_{OUT}/I_{OUT}$, the value of R_{equ_case2} is larger than that of case 1. Therefore, the above factors together with the actual requirements should be considered comprehensively in selecting these two cases.

F. COMPARISON OF THE TWO POSSIBLE CC DESIGN CASES

Take the application of the EV charger as an example, the G_v for the IPT system is usually below 1.5 while the G_i is below 0.1 [11], [12]. Therefore, G_v and G_i are set as 1.5 and 0.1 respectively as the design requirements for the cases study here. According to (25), the coupling coefficient of magnetic couplers, the square root of the self-inductance ratio, and the square root of the product of the self-inductance are selected as the benchmark for gain comparison. The G_v and G_i can be depicted as Fig. 5. Specifically, Fig. 5(a) illustrates that if case 1 is adopted, the targeted design value of G_v and G_i as highlighted lines can be obtained when the coupling coefficient is around 0.3. Fig. 5(b) illustrates that if case 2 is used, the expected value of G_i is found when the coupling coefficient is around 0.2. However, the expected value of G_v is not achievable since the minimum voltage gain is 4. Therefore, the case 1 is more suitable for the EV wireless charger while case 2 can be used in applications where high voltage gain is required.

G. VERIFICATION OF LOAD-INDEPENDENT CC AND CV MODES

To verify the required output characteristics, a typical IPT charging system with specifications listed as Table 2. has been taken as an example. All the parameters of the resonant tank can be calculated by the aforementioned design rules, which have been included in the captions of Fig. 6. In the case of varying frequency and different load, the curves of G_v , G_i , and phase angle of the input impedance Z_{IN} are drawn as Fig. 6(a), (b), and (c) respectively. It can be observed from

Fig. 6(a) that G_v is a constant at the CV frequency of 85kHz regardless of the load variation, while ZPA achieves shown as Fig. 6(c). Similarly, the G_i is a constant at the CC frequency of 106.1kHz regardless of the load variation and achieves ZPA.

III. PARAMETERS DESIGN PROCEDURE

A. INFLUENCE OF VARIOUS PARAMETERS ON THE INPUT IMPEDANCE ANGLE

It has been proved that the converter operates in ZPA condition when the resonant circuit parameters are designed in full compliance with the above rules. However, to decrease the switching loss, zero voltage switching (ZVS) operation is preferable than ZPA operation for a MOSFET based inverter. That is to say, the input impedance of the resonant tank driven by the inverter should be inductive. Therefore, the influence of each parameter on the input impedance should be analyzed to have the whole circuit maintain inductive in the entire charging process.

The input impedance angle (α) expression has been derived as (17). It is well-known that α is equal to zero when the circuit is resistive. Besides, positive α represents inductive input impedance, otherwise capacitive impedance.

For the sake of intuitively showing the impact of parameter variation, C^* , L^* and k^* is defined to represent the original value of C , L and k at resonance. Thus, the relationship between α and C_2 in CV mode can be simplified.

$$\alpha = \arctan\left(\frac{C_2/C_2^* - 1}{\omega_{CV} C_2 R_{OUT}}\right) \quad (26)$$

Similarly, according to the relationship between ω_{CV} and ω_{CC} in case 1, the phase α can be rewritten as

$$= \arctan\left(\frac{1 - C_2/C_2^*}{\omega_{CV} C_2 R_{OUT} \sqrt{1/(1-k)}}\right) \quad (27)$$

Accordingly, the influence of resonant network parameters on α is calculated and summarized in Table 3. It can be observed that when C_2 is larger than the resonance value, the circuit is always inductive in CC mode while remaining capacitive in CV mode. Therefore, adjusting C_2 cannot guarantee that the circuit remains inductive in the entire charging process. Besides, the impedance characteristic cannot be concluded directly from Table 3 when the capacitance of C_1 or C_{f1} is adjusted. Fortunately, increasing the value of L_{f1} can make the resonant tank inductive since the term of $(L_{f1} - L_{f1}^*)$ are identical in both CC and CV modes' impedance expression. Therefore, ZVS can be realized for the entire charging process by tuning L_{f1} .

$$Z_{inCC} = \frac{-\omega_{CV} L_{f1} (\alpha^6 \omega_{CV} (M^2 - L_1 L_2) + j \alpha^5 R_{OUT} L_1 - \alpha^4 \omega_{CV} (M^2 - 3L_1 L_2) - 2j \alpha^3 R_{OUT} L_1 - \alpha^2 \omega_{CV} L_2 (3L_1 - L_{f1}) + j \alpha R_{OUT} (L_1 - L_{f1}) + \omega_{CV} L_2 (L_1 - L_{f1}))}{\alpha (j \alpha^4 \omega_{CV} (M^2 - L_1 L_2) - \alpha^3 R_{OUT} L_1 + 2j \alpha^2 \omega_{CV} L_1 L_2 + \alpha R_{OUT} L_1 - j \omega_{CV} L_1 L_2)} \quad (22)$$

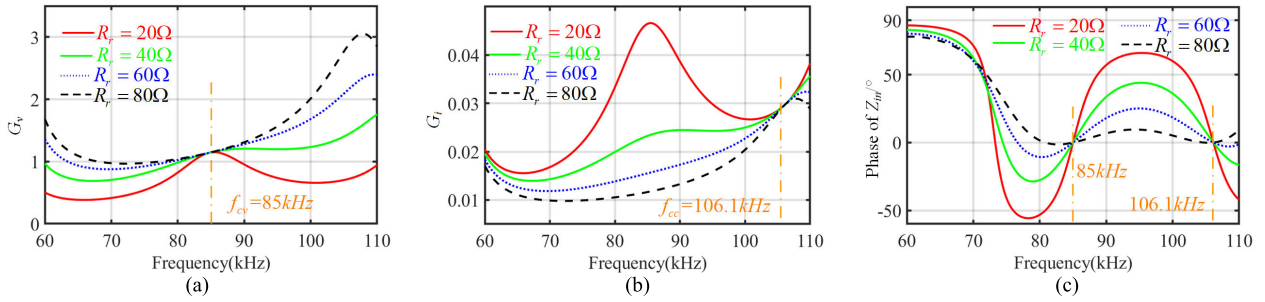


FIGURE 6. (a) G_v of the IPT converter. (b) G_i of the IPT converter. (c) Phase of Z_{in} . (When $L_1 = 252\mu F$, $L_2 = 244.6\mu F$, $L_{f1} = 75.7\mu F$, $C_{f1} = 44.54nC$, $C_1 = 20.23nC$ and $C_2 = 41.33nC$, $k = 0.3585$).

TABLE 3. The relationship between compensation network parameters and α .

Parameters	α in CV mode	α in CC mode
C_1	$\alpha = \arctan\left(\frac{(C_1^* - C_1)R_{OUT}}{\omega_{CV}^3 k^2 L_1 L_2 C_1 C_1^*}\right)$	$\alpha = \arctan\left(\frac{(C_1 - C_1^*)(2k - 1) \times A}{(k - 1)^3 k^3 R_{OUT} \omega_{CV} L_2 C_1^2 \sqrt{1/(1 - k)}}\right)$
C_2	$\alpha = \arctan\left(\frac{C_2 / C_2^* - 1}{\omega_{CV} C_2 R_{OUT}}\right)$	$\alpha = \arctan\left(\frac{1 - C_2 / C_2^*}{\omega_{CV} C_2 R_{OUT} \sqrt{1/(1 - k)}}\right)$
C_{f1}	$\alpha = \arctan\left(\frac{(C_{f1} / C_{f1}^* - 1) \times B}{\omega_{CV} M^2 R_{OUT}}\right)$	$\alpha = \arctan\left(\frac{(C_{f1}^* - C_{f1}) \times D}{\omega_{CV} C_{f1}^* L_2 R_{OUT} k^2 (k - 1)^3 \sqrt{1/(1 - k)}}\right)$
L_{f1}	$\alpha = \arctan\left(\frac{(L_{f1} - L_{f1}^*) k^2 L_1 L_2 \omega}{R_{OUT} L_{f1}^2}\right)$	$\alpha = \arctan\left(\frac{(L_{f1} - L_{f1}^*) R_{OUT}}{\omega_{CV} k^2 L_2 L_{f1} \sqrt{1/(1 - k)}}\right)$
k	$\alpha = 0$	$\alpha = \arctan\left(\frac{(k^{*2} - k^2) \omega_{CV} L_2}{k^* (k^* - 1) \sqrt{1/(1 - k^*)} R_{OUT}}\right)$

$$A = ((L_2^2 k^4 \omega_{CV}^2 + (R_{OUT}^2 - 3L_2^2 \omega_{CV}^2) k^3 + L_2^2 k^2 \omega_{CV}^2 - 2R_{OUT}^2 k + R_{OUT}^2) C_1 - (2k - 1)(R_{OUT}^2 k - R_{OUT}^2 - L_2^2 k^2 \omega_{CV}^2) C_1^*)$$

$$B = (\omega_{CV}^4 C_{f1} k^4 L_1^2 L_2^2 + R_{OUT}^2 C_{f1} / \omega_{CV}^2 C_{f1}^2 - 2R_{OUT}^2 / \omega_{CV}^2 C_{f1}^2)$$

$$D = (L_2^2 k^5 \omega_{CV}^2 C_{f1}^* + L_2^2 \omega_{CV}^2 k^4 (C_{f1} - 2C_{f1}^*) + R_{OUT}^2 k^2 C_{f1}^* - R_{OUT}^2 k (C_{f1} + C_{f1}^*) + R_{OUT} C_{f1})$$

B. ANALYSIS ON THE IMPACT OF TUNING PARAMETERS ON SYSTEM CHARACTERISTICS

In order to confirm the feasibility of the tuning method, the influence of parameter changes on the entire system is further analyzed. Firstly, based on the above-mentioned system parameters, the trend of the impedance angle of the system when each parameter is adjusted as shown in Fig. 7. It can be observed that in both CC and CV modes, a slight decrease of C_1 or the increase of L_{f1} will make the whole circuit inductive no matter in P_0 or $0.5P_0$. This is basically consistent with the aforementioned analysis. Therefore, by adjusting L_{f1} , it is possible to satisfy ZVS in CC and CV modes.

Secondly, since the output voltage and current play a vital role in the system, the influence caused by varying parameters also needs to be considered. The normalized output current and voltage with varying normalized parameters are shown in Fig. 8. It is quite clear that the change of C_1 has an insignificant influence on the gain of voltage while causing great influence on the gain of the current. In contrast, the varying

L_{f1} has a small effect on the output voltage and current. Therefore, ZVS can be realized by adjusting L_{f1} to ensure that the overall performance is not greatly affected. It should be noted that a very wide range of ZVS can be achieved by offsetting the L_{f1} in a large value, and the transmission characteristics of the system will be affected non-negligibly. When considering the ZVS range, it needs to be related to the fluctuation of the transmission characteristics. It is essential to consider them together and make a trade-off before selecting the parameters.

C. PARAMETER TUNING OF ZVS AND SYSTEM DESIGN PROCESS

Specifically, to guarantee ZVS operation in both modes, the turn-off current of MOSFET must be large enough to discharge the junction capacitors within the dead-time, which can be expressed as follows: [34]

$$I_{OFF} \geq \frac{4C_{OSS}U_{AB,max}}{t_d} \tag{28}$$

TABLE 4. Compensation circuit parameter for the proposed system.

Parameters	Simulation	Measurement
Lize wire(strand diameter, N. of strands)	0.1mm 1500	0.1mm 1500
Outer diameters and turns of the primary winding	550mm*500mm 11	550mm*500mm 11
Outer diameters and turns of the secondary winding	550mm*500mm 11	550mm*500mm 11
Air Gap	120mm	120mm
Self-inductance of primary coil L_1	252 μ H	246.38 μ H
Self-inductance of secondary coil L_2	244.6 μ H	249.3 μ H
Coupling coefficient k	0.3585	0.349
Resonant frequency f_{cv} and f_{cc}	85kHz, 106.126kHz	85kHz, 105.5kHz
Primacy compensation inductor L_{f1}	78.7 μ H	75.8 μ H
Primary parallel compensation capacitor C_{f1}	44.54nF	49.51nF
Primary compensation capacitor C_1	20.23nF	19.97nF
Secondary compensation capacitor C_2	14.33nF	14.06nF

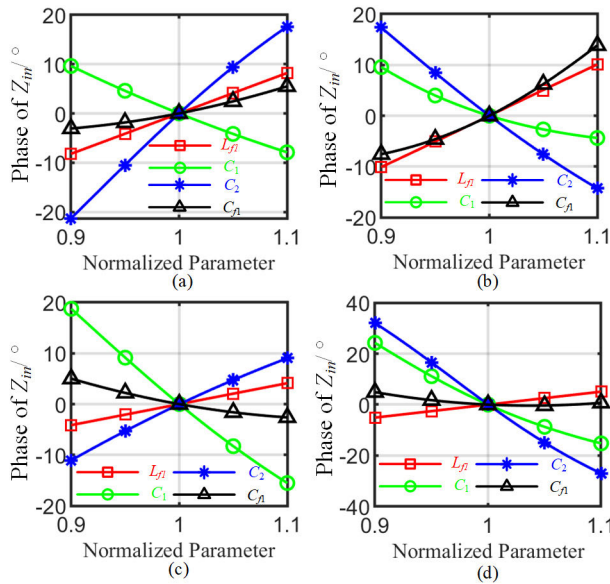


FIGURE 7. Phase angle of input impedance versus normalized parameters (a) CV mode: $P_{out} = P_0$ (b) CC mode: $P_{out} = P_0$ (c) CV mode: $P_{out} = 0.5P_0$ (d) CC mode: $0.5P_0$.

where C_{oss} is the junction capacitance, $U_{AB,max}$ is the max input voltage, and t_d is the dead time.

In order to analyze the current at the switching time more accurately, it is necessary to further calculate the influence of high-order harmonics. As stated in [11], for high-order harmonics calculation, the interaction between the primary and secondary sides can be ignored because the couplers can be regarded as a high-order filter. Moreover, the sum of the value of high-order harmonics at the switching time can be expresses as:

$$I_{OFF_high_order} = \frac{\sqrt{2} U_{AB}}{4 \omega L_{f1}} \quad (29)$$

After combining the influence of high-order harmonics and the fundamental wave, the required tuning value of L_{f1} can be

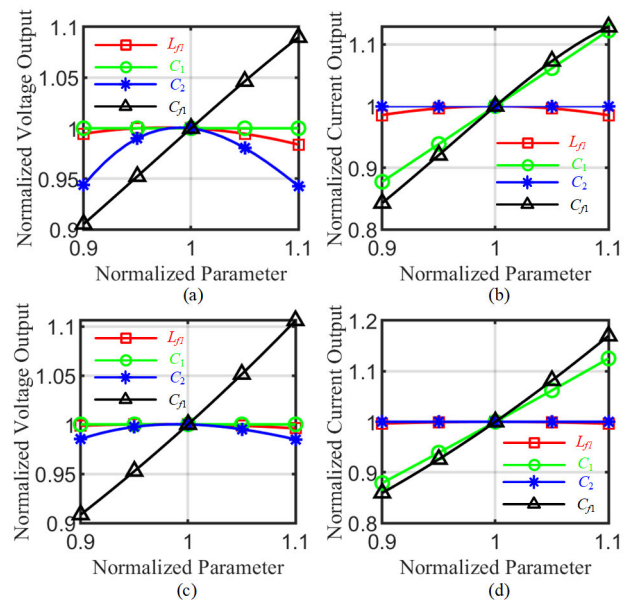


FIGURE 8. Normalized output with varying normalized parameters (a) CV mode: $P_{out} = P_0$ (b) CC mode: $P_{out} = P_0$ (c) CV mode: $P_{out} = 0.5P_0$ (d) CC mode: $0.5P_0$.

solved by the following formula:

$$I_{OFF} - I_{OFF_high_order} = I_{IN} \sin \alpha \quad (30)$$

To sum up, a practical parameter design procedure is summarized as Fig. 9 for the LCC-S compensated IPT charging system to realize the CC charge with subsequent CV charge profile. First of all, the resonant frequency of the CV mode f_{CV} is selected by considering the volume and the loss of the resonant components [3]. Next, the size of the magnetic coupler is affected by the parameter limitation in the targeted application. The value of L_1, L_2 and k can be obtained by using electromagnetic field analysis software. Then L_{f1} and f_{CC} can be determined by using (25). The value of, C_1, C_2 , and C_{f1} can be calculated by using (18) respectively. Then, an LCC-S compensated IPT charger can realize input ZPA

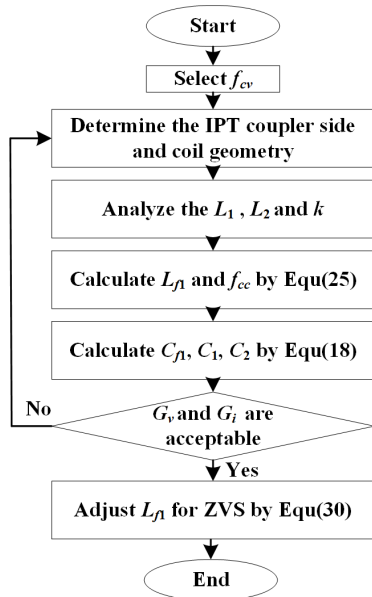


FIGURE 9. Design procedure of the proposed IPT charger.

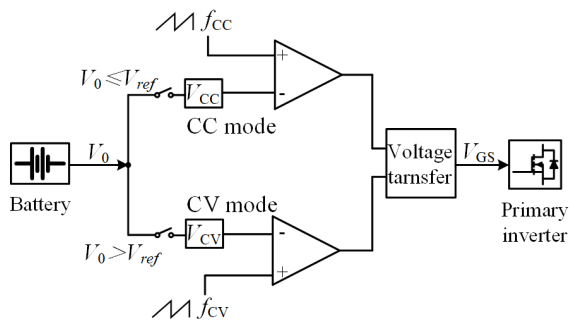


FIGURE 10. Schematic of switching module for IPT charger.

with both output CC or CV mode by changing the operation frequency. Last but not least, by weighing the ZVS range as well as the output characteristic fluctuations, the final adjustment value of L_{f1} is derived by equation (30).

IV. EXPERIMENTAL VALIDATION

According to the proposed design procedure, the tuned value of L_{f1} for ZVS operation can be calculated based on the previously designed IPT charger as shown in Fig. 9. Besides, a prototype has been built to verify the theoretical analysis of the expected load-independent CC and CV characteristics with ZVS realization. All the designed parameters and actual measurement parameters of the prototype can be founded in Table 4. When constructing the prototype, the current and voltage stress of the components can be obtained by (7,10, 12, 25), and the selection of components is carried out accordingly to ensure the reliability of the system.

Varying frequency should be adjusted according to the charging mode in practical situation. Therefore, it is necessary to adopt the switching module to achieve the CC and CV mode transition. As shown in Fig. 10, the charging mode

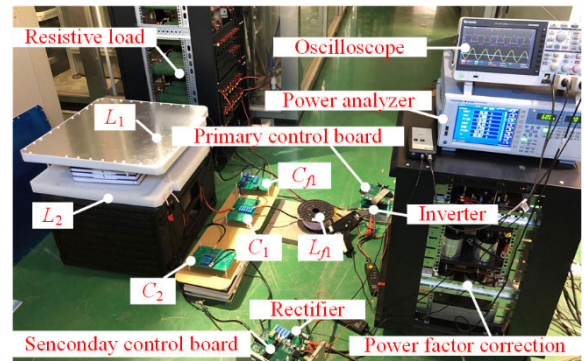


FIGURE 11. Experimental Setup for LCC-S IPT charger.

depends on the feedback signal of battery voltage V_0 . When the battery voltage is lower than the preset voltage V_{ref} , 400V in this paper, the switching of the current mode is activated. Once the voltage of battery exceeds 400V, the current mode is switched OFF, and the voltage module is switched ON.

The experimental setup is shown in Fig. 11. The full-bridge inverter is composed of four MOSFETs (C2M0040120D), and the secondary rectifier uses fast-recovery diodes (C5D50065D). The output filter capacitor is $10\mu\text{F}$. Moreover, multiple capacitors in parallel are adopted to acquire the voltage and current rating of the LCC-S compensation tank. Texas Instruments Incorporated TMS320F28335 DSP is used to implement closed-loop control. The battery voltage and current are separately measured by LV-25P voltage sensor and HO 25-P/SP33 n current sensor. The sensed signal of the secondary side can be feedback wirelessly with no difficulty by using a mature module (NRF24L01). A resistive load is used to emulate the battery. Besides, the waveforms of the circuit are captured by Tektronix TBS 2000.

As mentioned in Table 2, an 8.75A charging current is required for CC mode until the output voltage reaches 400V for the fabricated prototype. Then 400V should be maintained in the whole CV mode. It means that the equivalent load resistance increases as the charging process proceeds. Fig. 12 shows the measured waveforms of input voltage U_{AB} , input current I_{AB} and the output current I_0 during CC mode charge in 105.5kHz for two values of load resistance R_r being 25Ω and 46Ω . It can be seen that the output current is maintained at about 8.7A although the loads is varying. When R_r arrives at 46Ω , V_0 is grown to 400V, and the charging mode needs to be switched to CV mode. Fig. 13 shows the frequency switching from f_{cc} to f_{cv} , which means that the driving signal of H-bridge inverter switches from 105.5kHz to 85kHz. It can be seen that the output voltage U_0 and output current I_0 change slightly during the switching moment. The waveforms of U_{AB} , I_{AB} , and U_0 in CV mode are shown in Fig. 14(a) and (b) while the R_r being 46Ω and 90Ω . However, the charging voltage of the battery changes slightly in different R_r . Furthermore, the V_{gs2} and V_{ds2} are provided to clearly show the ZVS operation. It can be seen that the ZVS

TABLE 5. Comparison of the proposed method and other related work.

Articles aiming at implementing CC and CV	[21]	[17]	[26]	[31]	[35]	[30]	This work
Number of transmitter-side compensation components	1	3	3	3	4	3	3
Number of receiver-side compensation components	1	4	3	3	1	1	1
Number of DC-DC converters	1	0	0	0	0	0	0
Number of active switches	5	6	4	4	4	4	4
ZPA in CC and CV mode	YES	YES	YES	NO	YES	YES	YES
Analysis of ZVS in CC and CV mode	NO	YES	YES	NO	NO	NO	YES
Terseness and rationality of system design	NO	YES	YES	NO	YES	NO	YES
Max Power	3.25kW	3.3kW	24W	3.5kW	144W	3.3kW	3.5kW
Peak efficiency	88.05%	91.8%	≈93%	92.9%	94%	90.8%	97.3%

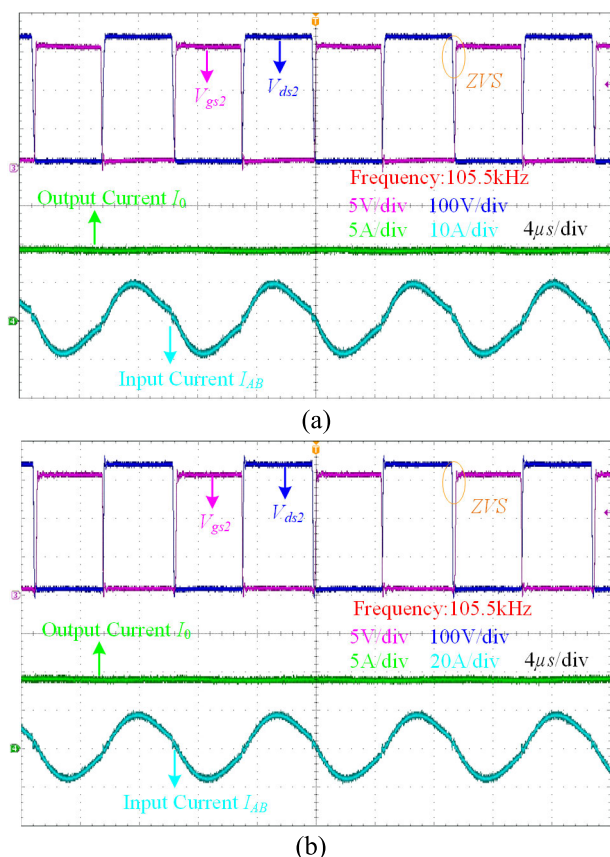


FIGURE 12. Experimental waveforms of I_{AB} , U_{AB} , I_0 in CC mode in the operation of different R_r (a) 25Ω (b) 46Ω .

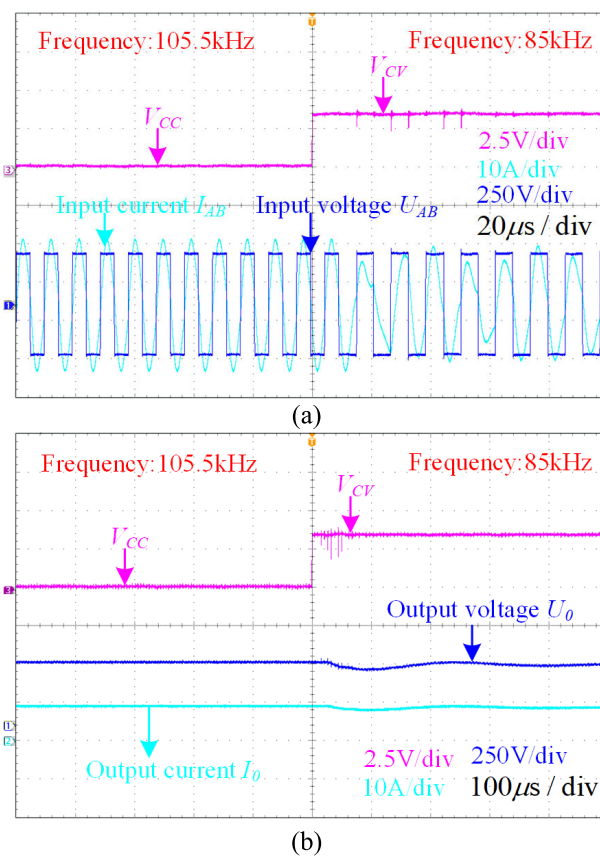


FIGURE 13. Experimental waveforms for switching from CC mode to CV mode (a) I_{AB} , U_{AB} (b) I_0 , U_0 .

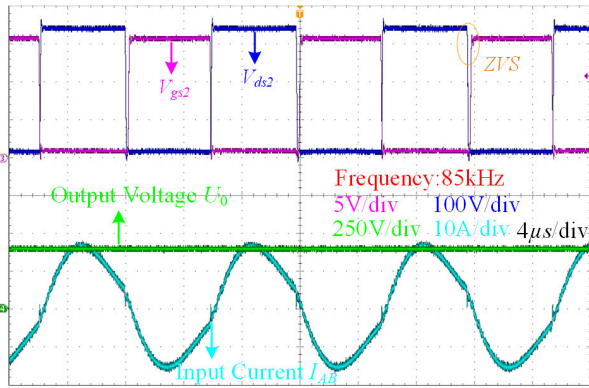
is achieved in both CC and CV mode, given low switching stresses and high transfer efficiency.

The entire charging process is shown in Fig. 15. The experimental data are consistent with the simulation data, which proves the validity of the parameter design. The efficiency of the whole charging process measured by YOKOGAWA WT1800 is plotted in Fig. 16. It shows that the efficiency is increasing with the output power in CC mode while the efficiency has been above 97% in CV mode. Furthermore, the efficiency improved at the switching point due to the smaller current flowing through the resonant tank in CV mode as a result of impedance changing in varying frequencies. Due to the change of input current, the loss ratio of each

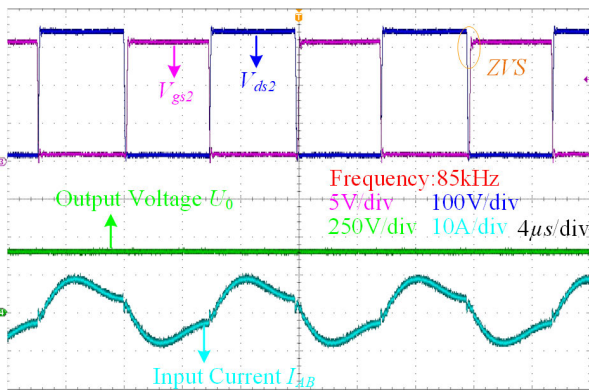
component is also different in CC and CV mode. As shown in Fig. 17, the higher primary current makes the ratio of copper loss and core loss larger in CC mode than CV mode.

Based on the above experimental results, the proposed method can achieve high efficient load-independent current or voltage characteristic output. In addition, a series of comparisons among the proposed method and recently related methods in the literature are made, and the results are listed in Table 5.

Firstly, compared with [17], [21], it is seen that the proposed method reduces the usage of active switches, avoids the introduction of a DC-DC transformer at the back end, therefore effectively reduces the complexity of system



(a)



(b)

FIGURE 14. Experimental waveforms of I_{AB} , U_{AB} , U_0 in CV charging mode and R_r of (a) 46Ω (b) 90Ω .

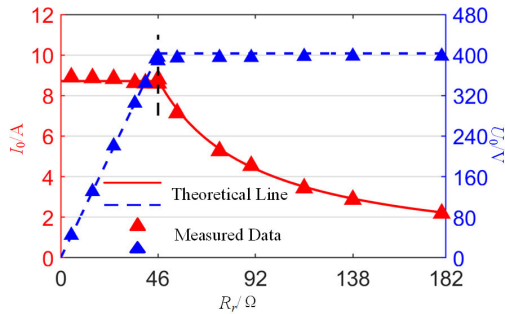


FIGURE 15. Measured charging process versus the equivalent battery load.

control. Secondly, the compensated components are significantly reduced, in this regard, which is beneficial to the lightweight of the receiver compared to [26], [31]. Thirdly, The proposed method clearly points out the parameter relationship between the gains and the couplers, which makes the design method simpler and more effective contrast to [30]. Fourthly, different from [30], [35], the parameter tuning object and its numerical calculation method to realize ZVS are proposed, making the system to work more efficiently. Last but not least, different from the articles listed above which operation efficiency in the entire CC-CV charging

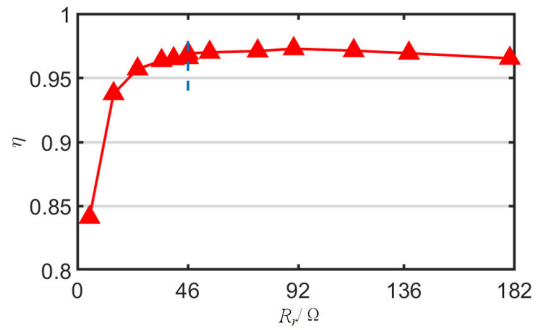


FIGURE 16. Experimental efficiency of the charging process.

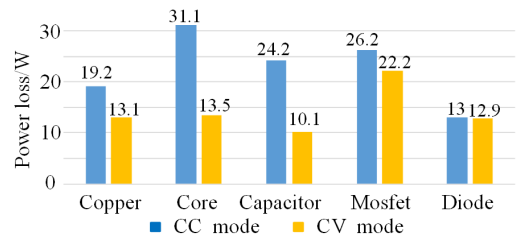


FIGURE 17. Power loss calculation of CC and CV mode in the operation of $R_r = 46\Omega$.

process is lower than 94%, the efficiency of the designed prototype maintains above 95% in a wide load range. In short, the proposed approach reduces the number of components required to achieve the CC-CV characteristics of the wireless charging system and simplifies the calculation process, thus reducing the cost and complexity of the system, at the same time, the conditions for achieving ZVS are proposed which improves the efficiency of the system charging process.

V. CONCLUSION

Focused on LCC-S compensation topology for wireless battery charging application, it is feasible to realize load-independent CC output and CV output characteristics respectively at different resonant frequencies. Usually, a specific resonant frequency defined by clear parameter constraints can be designed first for CV output mode with ZPA operation. Subsequently, two load-independent resonant frequencies can be found by analytical expressions for achieving CC output mode with ZPA operation. The two CC mode operation frequencies hold different characteristics in terms of voltage gain and transconductance gain, which needs to be selected properly according to the actual scenarios. Although the CC frequency is inconsistent with the usual resonance frequency, it ensures the realization of ZPA, which can also achieve high efficiency. Besides, it is found that the preferable ZVS operation for the MOSFET-based inverter can be achieved in a wide operating range by tuning the primary compensated inductance. A comprehensive parameter design procedure has been summarized for LCC-S compensation topology to have both load-independent CC and CV output while ZVS operation is guaranteed. The great performance of

the proposed parameter design method in its high efficiency and feasibility has been validated by experiments.

REFERENCES

- [1] S. Y. Hui, "Planar wireless charging technology for portable electronic products and Qi," *Proc. IEEE*, vol. 101, no. 6, pp. 1290–1301, Jun. 2013.
- [2] C. Xiao, D. Cheng, and K. Wei, "An LCC-C compensated wireless charging system for implantable cardiac pacemakers: Theory, experiment, and safety evaluation," *IEEE Trans. Power Electron.*, vol. 33, no. 6, pp. 4894–4905, Jun. 2018.
- [3] S. Li and C. C. Mi, "Wireless power transfer for electric vehicle applications," *IEEE J. Emerg. Sel. Topics Power Electron.*, vol. 3, no. 1, pp. 4–17, Mar. 2015.
- [4] C. C. Mi, G. Buja, S. Y. Choi, and C. T. Rim, "Modern advances in wireless power transfer systems for roadway powered electric vehicles," *IEEE Trans. Ind. Electron.*, vol. 63, no. 10, pp. 6533–6545, Oct. 2016.
- [5] S. M. Lukic, J. Cao, R. C. Bansal, F. Rodriguez, and A. Emadi, "Energy storage systems for automotive applications," *IEEE Trans. Ind. Electron.*, vol. 55, no. 6, pp. 2258–2267, Jun. 2008.
- [6] M. A. Hannan, M. M. Hoque, A. Hussain, Y. Yusof, and P. J. Ker, "State-of-the-art and energy management system of lithium-ion batteries in electric vehicle applications: Issues and recommendations," *IEEE Access*, vol. 6, pp. 19362–19378, 2018.
- [7] J. Deng, C. C. Mi, R. Ma, and S. Li, "Design of LLC resonant converters based on operation-mode analysis for level two PHEV battery chargers," *IEEE/ASME Trans. Mechatronics*, vol. 20, no. 4, pp. 1595–1606, Aug. 2015.
- [8] J. Deng, J. Deng, W. Li, S. Li, and C. Mi, "Magnetic integration of LCC compensated resonant converter for inductive power transfer applications," in *Proc. IEEE Energy Convers. Congr. Expo. (ECCE)*, Sep. 2014, pp. 660–667.
- [9] C.-S. Wang, G. A. Covic, and O. H. Stielau, "Power transfer capability and bifurcation phenomena of loosely coupled inductive power transfer systems," *IEEE Trans. Ind. Electron.*, vol. 51, no. 1, pp. 148–157, Feb. 2004.
- [10] Z. Pantic, S. Bai, and S. M. Lukic, "ZCS LCC-compensated resonant inverter for inductive-power-transfer application," *IEEE Trans. Ind. Electron.*, vol. 58, no. 5, pp. 3500–3510, Aug. 2011.
- [11] S. Li, W. Li, J. Deng, T. D. Nguyen, and C. C. Mi, "A double-sided LCC compensation network and its tuning method for wireless power transfer," *IEEE Trans. Veh. Technol.*, vol. 64, no. 6, pp. 2261–2273, Jun. 2015.
- [12] W. Zhang and C. C. Mi, "Compensation topologies of high-power wireless power transfer systems," *IEEE Trans. Veh. Technol.*, vol. 65, no. 6, pp. 4768–4778, Jun. 2016.
- [13] R. Mai, Y. Chen, Y. Zhang, N. Yang, G. Cao, and Z. He, "Optimization of the passive components for an S-LCC topology-based WPT system for charging massive electric bicycles," *IEEE Trans. Ind. Electron.*, vol. 65, no. 7, pp. 5497–5508, Jul. 2018.
- [14] X. Qu, H. Han, S.-C. Wong, C. K. Tse, and W. Chen, "Hybrid IPT topologies with constant current or constant voltage output for battery charging applications," *IEEE Trans. Power Electron.*, vol. 30, no. 11, pp. 6329–6337, Nov. 2015.
- [15] C. Auvigne, P. Germano, D. Ladas, and Y. Perriard, "A dual-topology ICPT applied to an electric vehicle battery charger," in *Proc. 20th Int. Conf. Electr. Mach.*, Sep. 2012, pp. 2287–2292.
- [16] R. Mai, Y. Chen, Y. Li, Y. Zhang, G. Cao, and Z. He, "Inductive power transfer for massive electric bicycles charging based on hybrid topology switching with a single inverter," *IEEE Trans. Power Electron.*, vol. 32, no. 8, pp. 5897–5906, Aug. 2017.
- [17] D. Wang, X. Qu, Y. Yao, and P. Yang, "Hybrid inductive-power-transfer battery chargers for electric vehicle onboard charging with configurable charging profile," *IEEE Trans. Intell. Transp. Syst.*, vol. 22, no. 1, pp. 592–599, Jan. 2021.
- [18] G. Buja, M. Bertoluzzo, and K. N. Mude, "Design and experimentation of WPT charger for electric city car," *IEEE Trans. Ind. Electron.*, vol. 62, no. 12, pp. 7436–7447, Dec. 2015.
- [19] A. Berger, M. Agostinelli, S. Vesti, J. A. Oliver, J. A. Cobos, and M. Huemer, "A wireless charging system applying phase-shift and amplitude control to maximize efficiency and extractable power," *IEEE Trans. Power Electron.*, vol. 30, no. 11, pp. 6338–6348, Nov. 2015.
- [20] Z. Huang, S. C. Wong, and C. K. Tse, "Design of a single-stage inductive-power-transfer converter for efficient EV battery charging," *IEEE Trans. Veh. Technol.*, vol. 66, no. 7, pp. 5808–5821, Jul. 2017.
- [21] Z. Li, C. Zhu, J. Jiang, K. Song, and G. Wei, "A 3-kW wireless power transfer system for sightseeing car supercapacitor charge," *IEEE Trans. Power Electron.*, vol. 32, no. 5, pp. 3301–3316, May 2017.
- [22] C. Zheng, J.-S. Lai, R. Chen, W. E. Faraci, Z. U. Zahid, B. Gu, L. Zhang, G. Lisi, and D. Anderson, "High-efficiency contactless power transfer system for electric vehicle battery charging application," *IEEE J. Emerg. Sel. Topics Power Electron.*, vol. 3, no. 1, pp. 65–74, Mar. 2015.
- [23] Q. Chen, S. C. Wong, C. K. Tse, and X. Ruan, "Analysis, design, and control of a transcutaneous power regulator for artificial hearts," *IEEE Trans. Biomed. Circuits Syst.*, vol. 3, no. 1, pp. 23–31, Feb. 2009.
- [24] X. Qu, Y. Jing, H. Han, S.-C. Wong, and C. K. Tse, "Higher order compensation for inductive-power-transfer converters with constant-voltage or constant-current output combating transformer parameter constraints," *IEEE Trans. Power Electron.*, vol. 32, no. 1, pp. 394–405, Jan. 2017.
- [25] V.-B. Vu, D.-H. Tran, and W. Choi, "Implementation of the constant current and constant voltage charge of inductive power transfer systems with the double-sided LCC compensation topology for electric vehicle battery charge applications," *IEEE Trans. Power Electron.*, vol. 33, no. 9, pp. 7398–7410, Sep. 2018.
- [26] X. Qu, H. Chu, S.-C. Wong, and C. K. Tse, "An IPT battery charger with near unity power factor and load-independent constant output combating design constraints of input voltage and transformer parameters," *IEEE Trans. Power Electron.*, vol. 34, no. 8, pp. 7719–7727, Aug. 2019.
- [27] Y. Wang, H. Wang, T. Liang, X. Zhang, D. Xu, and L. Cai, "Analysis and design of an LCC/S compensated resonant converter for inductively coupled power transfer," in *Proc. IEEE Transp. Electrific. Conf. Expo. Asia-Pacific (ITEC Asia-Pacific)*, Aug. 2017, pp. 1–5.
- [28] J. Yang, X. Zhang, K. Zhang, X. Cui, C. Jiao, and X. Yang, "Design of LCC-S compensation topology and optimization of misalignment tolerance for inductive power transfer," *IEEE Access*, vol. 8, pp. 191309–191318, 2020.
- [29] J. Lu, G. Zhu, W. Li, and B. Li, "Load-independent ZPA conditions in both constant current and constant voltage modes of LCC-series compensated IPT system," in *Proc. IEEE Wireless Power Transf. Conf. (WPTC)*, Jun. 2018, pp. 1–4.
- [30] J. Lu, G. Zhu, D. Lin, Y. Zhang, J. Jiang, and C. C. Mi, "Unified load-independent ZPA analysis and design in CC and CV modes of higher order resonant circuits for WPT systems," *IEEE Trans. Transport. Electrific.*, vol. 5, no. 4, pp. 977–987, Dec. 2019.
- [31] J. Lu, G. Zhu, D. Lin, S.-C. Wong, and J. Jiang, "Load-independent voltage and current transfer characteristics of high-order resonant network in IPT system," *IEEE J. Emerg. Sel. Topics Power Electron.*, vol. 7, no. 1, pp. 422–436, Mar. 2019.
- [32] M. Borage, S. Tiwari, and S. Kotaiah, "Analysis and design of an LCL-T resonant converter as a constant-current power supply," *IEEE Trans. Ind. Electron.*, vol. 52, no. 6, pp. 1547–1554, Dec. 2005.
- [33] A. Ramezani, S. Farhangi, H. Iman-Eini, B. Farhangi, R. Rahimi, and G. R. Moradi, "Optimized LCC-series compensated resonant network for stationary wireless EV chargers," *IEEE Trans. Ind. Electron.*, vol. 66, no. 4, pp. 2756–2765, Apr. 2019.
- [34] B. Lu, W. Liu, Y. Liang, F. C. Lee, and J. D. Van Wyk, "Optimal design methodology for LLC resonant converter," in *Proc. IEEE Appl. Power Electron. Conf. Expo. (APEC)*, Mar. 2006, pp. 533–538.
- [35] L. Yang, X. Li, S. Liu, Z. Xu, and C. Cai, "Analysis and design of an LCCC/S-compensated WPT system with constant output characteristics for battery charging applications," *IEEE J. Emerg. Sel. Topics Power Electron.*, vol. 9, no. 1, pp. 1169–1180, Feb. 2021.



WENBO WANG was born in Jiangxi, China, in 1996. He received the B.S. degree in automotive engineering from Hunan University, Hunan, China, in 2018. He is currently pursuing the Ph.D. degree in mechanical engineering with the National Engineering Laboratory for Electric Vehicles, Beijing Institute of Technology.

His research interests include inductive power transfer and resonant converters.



JUNJUN DENG (Member, IEEE) received the B.S., M.S., and Ph.D. degrees in electrical engineering from Northwestern Polytechnical University, Xi'an, China, in 2008, 2011, and 2015, respectively.

From 2011 to 2014, he was a Visiting Scholar with the Department of Electrical and Computer Engineering, University of Michigan–Dearborn, Dearborn, MI, USA. In 2016, he joined the Faculty of Vehicle Engineering, Beijing Institute of Technology, Beijing, China. His research interests include wireless power transfer, resonant power conversion, and high performance battery chargers for electric vehicles.



DELIANG CHEN was born in Fujian, China, in 1994. He received the B.S. and M.S. degrees in electrical engineering from Beijing Institute of Technology (BIT), Beijing, China, in July 2016 and July 2019, respectively, where he is currently pursuing the Ph.D. degree in mechanical engineering.

His research interests include high frequency and high efficiency DC/DC power conversion, solid state transformer, and wireless power transfer.



ZHENPO WANG received the B.Eng. degree from Tongji University and the Ph.D. degree in automotive engineering from Beijing Institute of Technology, Beijing, China, in 2005.

He is currently a Professor with Beijing Institute of Technology and the Director of the National Engineering Laboratory for Electric Vehicles. He has published four monographs and translated books as well as more than 80 technical papers. He holds more than 60 patents. His current research interests include pure electric vehicle integration, packaging and energy management of battery systems, and charging station design.

Prof. Wang was a recipient of numerous awards, including the Second National Prize for Progress in Science and Technology and the First Prize for Progress in Science and Technology from the Ministry of Education, China, and the Second Prize for Progress in Science and Technology from Beijing Municipal, China.



SHUO WANG (Member, IEEE) received the B.S. degree in electrical engineering from Shandong University of Science and Technology, Qingdao, China, in 2009, the M.S. degree in electrical engineering from China University of Mining and Technology, Beijing, China, in 2012, and the Ph.D. degree in engineering from the Faculty of Engineering and Information Technology (FEIT), University of Technology Sydney, in 2017.

He was a Postdoctoral Research Fellow with Beijing Institute of Technology, from 2017 to 2021. He is currently an Assistant Professor with Beijing Institute of Technology, Beijing. His research interests include wireless charging, electric vehicle, and big data analysis.

...